Evaluation of ocean tide models used for Jason-2 altimetry corrections

H.S. Fok[1], H. Baki Iz[2], C.K. Shum[1], Yuchan Yi[1], Ole Andersen[3], Alexander Braun[4], Yi Chao[5], Guoqi Han[6], C.Y. Kuo[7], Koji Matsumoto[8], Y. Tony Song[5]

[1]Division of Geodetic Science, School of Earth Sciences, Ohio State University (125 South Oval Mall, 275 Mendenhall Lab., Columbus, Ohio 43210, USA, fok.8@buckeyemail.osu.edu, ckshum@osu.edu, yi.3@osu.edu)
[2]Dept. of Land Surveying and Geo-Informatics, Hong Kong Polytechnic University (Hung Hom, Kowloon, Hong Kong, lshbiz@polyu.edu.hk)
[3]Division of Geodesy, The National Space Institute, Technical University of Denmark (Juliane Maries Vej 30, DK-2100 Copenhagen, Denmark, oa@space.dtu.dk)
[4]Dept. Of Geosciences, School of Natural Sciences and Mathematics, University of Texas at Dallas (800 West Campbell Road, Richardson, Texas 75080, USA, braun@utdallas.edu)
[5]Jet Propulsion Laboratory, California Institute of Technology (M/S 300-323, 4800 Oak Grove Drive, Pasadena, CA, 91109, USA, Yi.Chao@jpl.nasa.gov, tony.song@jpl.nasa.gov)
[6]Northwest Atlantic Fisheries Centre, Fisheries and Oceans Canada (St. John's, Newfoundland, Canada, Guoqi.Han@dfo-mpo.gc.ca)
[7]Dept. of Geomatics, National Cheng Kung University (No.1, University Road, Tainan 701, Taiwan, Kuo70@mail.ncku.edu.tw)
[8]RISE Project, National Astronomical Observatory of Japan (2-12, Hoshigaoka, Mizusawa, Oshu, Iwate 023-0861, Japan, matumoto@miz.nao.ac.jp)

ABSTRACT

It has been over a decade since the last comprehensive accuracy assessment of global ocean tide models. Here, we conduct an evaluation of the barotropic ocean tide corrections, which were computed using FES2004 and GOT00.2, and other models, on the Jason-2 altimetry Geophysical Data Record (GDR), with a focus on selected coastal regions with energetic ocean dynamics. We compared 9 historical and contemporary ocean tide models with pelagic tidal constants, and with multiple satellite altimetry mission (T/P, ERS-1/-2, Envisat, GFO, Jason-1/-2) sea level anomalies using variance reduction studies. All accuracy assessment methods show consistent results. We conclude that all the contemporary ocean tide models evaluated have similar performance in the selected coastal regions. However, their accuracies are region-dependent and overall are significantly worse than those in the

deep-ocean, which are at the 2–3 cm RMS (root-mean-square) level. The Gulf of Mexico and Northwest Atlantic regions present the least reduction of altimetry sea surface height variability after ocean tides are removed, primarily because of large oceanic variability associated with loop currents in the Gulf of Mexico and the Gulf Stream in the Northwest Atlantic.

Keywords: Ocean tides, Satellite altimetry, Coastal regions

1. INTRODUCTION

The advent of satellite radar altimetry, which was introduced in the 1970s, provided a means of observing the global ocean surface (and other surfaces) topographic heights synoptically with an approximately weekly temporal sampling, a cross-track resolution of ~100 km, and with an increasing accuracy. The beginning of the 1990s represents a new era of satellite altimetry with the launch of ERS-1 in 1991. The launch of TOPEX/POSEIDON, owing to its near-global coverage and unprecedented accuracy, optimal orbital sampling to minimize tidal and seasonal signal aliasing and adequate spatial and temporal sampling initiates the advent of satellite oceanography and tidal science using satellite altimetry [*Fu et al.,* 1994]. Since then, other missions, ERS-2, GFO, Envisat, Jason-1, Jason-2, have been launched to lengthen the geophysical and oceanographic time series, in particular for the study of ocean's role in climate change, including sea-level rise, general ocean circulation and heat transport.

The measurement and prediction of the amplitude and phase of ocean tides, which account for 80% variability in sea surface topography [*Ray,* 1993; *Le Provost et al.,* 1994], have been important for commerce and science for thousands of years [*Shum et al.,* 1997]. Tides also have strong influence on modeling of coastal or continental shelf circulations, contribute to the wobble of the Earth and change the length of day, dissipate their energy in the ocean and solid Earth, and decelerate the Moon's mean motion. Ocean tides also play a significant role

in climate due to its complex interactions between ocean, atmosphere, and sea ice. The knowledge of prediction of barotropic ocean tides also serves as a critical correction for spaceborne measurements, directly as a geometric correction for the satellite altimetry data, or indirectly modeled as orbital perturbation on the spaceborne gravity sensors, such as GRACE and GOCE [*Bosch et al*., 2009], to enable improved quantification of general ocean circulation [*Fu and Cazenave*, 2001] and Earth's climate-sensitive signals of mass variations or transport.

The accurate prediction of ocean tides is of especially critical importance for coastal applications. Examples include, but are not limited to, operational ocean [*Han et al*., 2010] and climate forecast [*Escudier & Fellous*, 2009], co-tidal chart generation for mariners [*Fang et al.*, 2004], study of regional tidal dynamics and dissipation [*Han*, 2000; *Zu et al*., 2008], and regional dynamics of the solid Earth through GPS and gravimeter data in which ocean loading tide derived from the major tidal constituents are a substantial correction component [*Inazu et al*., 2009; *Yuan et al*., 2009]. Most of the abovementioned applications rely heavily on the global ocean tide model as initial boundary conditions for regional studies.

While ocean tides derived from satellite altimetry in the deep ocean are known to within 2 to 3 cm RMS accuracy, their uncertainties inflate significantly near coastal regions or over shallow seas [*Shum et al*., 1997, 2001], and even for the most recent models [*Ray*, 2009]. This is attributed to local hydrodynamic processes and bathymetry over different regions, which are subject to further regional modeling and investigation. *Lyard et al.* (2009) provides an alternative assessment on internal error estimates of major tidal constituents by taking into consideration the changes of barotropic tides estimated from along-track response analysis through crossover analysis of each tidal constituent, whereas conventional analysis is based on reference ground truth data and altimetry sea level time series variance reduction.

It has been over a decade since the last comprehensive accuracy assessment of the predictability of global ocean tide models [*Shum et al.*, 1997]. Since then a number of contemporary, improved ocean tide models have been developed. This study assesses and validates the performance of barotropic ocean tide corrections – computed from FES2004 and GOT00.2 models – used in Jason-2 altimeter Geophysical Data Record (GDR), as well as other ocean tide models. Here, we conduct accuracy assessments of 9 ocean tide models including the Jason-2 GDR models, FES2004 and GOT00.2, focusing on selected coastal ocean regions, in which tides are much less well known than in the deep ocean [*Shum et al*., 2001; *Ray*, 2009]. We compare ocean tide models with pelagic tidal constants derived from tide gauges or ocean bottom pressure gauges, and use them as corrections (computed in terms of geocentric tides which are the sum of pure ocean tides and load tides due to self-gravitation) to infer multiple satellite altimetry mission sea level anomalies, to assess the respective accuracy of each of the tide models. In addition to the accuracy assessment of contemporary ocean tide models in coastal regions, the study is anticipated to provide an estimate of magnitude of residual sea surface anomaly variability in various coastal regions of the world, providing an incentive to further improve ocean tide models and to separate tides from oceanic variability.

2. CONTEMPORARY OCEAN TIDE MODELS

GOT00.2 and FES2004 are the default ocean tide models used to compute tide corrections in the Jason-2 Geophysical Data Records (GDR) [*Dumont et al.*, 2008]. GOT00.2, based on FES94.1 and several other local hydrodynamic models as a-priori model, is an empirical model made by using 286 cycles (10-day exact repeat orbital cycles) of TOPEX data (covering the global ocean within $\pm 66^0$ latitude bounds), complemented by 81 cycles (35-day repeat orbital cycles) of ERS-1 and ERS-2 data in shallow seas and in polar ocean covering latitudes in between $\pm 81.5^0$ [*Ray*, 1999]; whereas FES2004 is a finite-element hydrodynamic model

constrained using data from tide gauges, TOPEX, ERS-1 and ERS-2 altimetry [*Lyard et al*., 2006].

Six other ocean tide models are also used in this study to validate their respective performance over the coastal regions: EOT08a [*Savcenko & Bosch*, 2008], GOT4.7 [*Ray*, 1999], NAO.99b [*Matsumoto et al*,, 2000], TPXO6.2, TPXO7.1, and TPXO7.2 [*Egbert & Erofeeva*, 2002]. Since most of the above models, except NAO.99b, are generated based on either a-priori ocean tide model with built-in hydrodynamics and the addition of altimeter data or the assimilation of tide gauge and altimeter data, a purely empirical multi-satellite tide solution is also included in the comparison.

Finally, a purely empirical tidal solution (OSU-NAO preliminary ocean tide model, denoted OSU06) [*Yi et al.*, 2006; *Shum et al*., 2006] is also used in the model evaluation study. OSU06 is developed using a modified orthotide tidal analysis [*Andersen*, 1994] in which eight dominant short-period tides and four long-period tides (i.e. annual, semi-annual, Mf and Mm) along with a bias term corresponding to each satellite track are simultaneously estimated [*Yi et al*., 2006; *Shum et al*., 2006]. The sea surface height (SSH) anomaly GDR data from TOPEX cycles 4–364, TOPEX Tandem Mission (TTM) cycles 369–479, Jason-1 version b cycles 1–221, GFO cycles 37–204, and Envisat cycles 10–61 were included to generate the solution, with a focus on coastal regions. Preprocessing of those data were made through the updates and retrieval of the so-called *stackfile* system in which the data are gradient-corrected, edited and post-processed [*Kruizinga*, 1997]. The standard deviations of the data are postulated as 3 cm (for TOPEX and Jason-1 version b), 6 cm (for GFO) and 8 cm (for Envisat) respectively, and were used for relative data weights for each of the data sets in the least squares tidal solution. To mitigate the tidal aliasing error and improve spatial coherence, those above data whose ground tracks fall within a predefined square area of $0.75^{o} \times 0.75^{o}$

were included to generate the corresponding solution at the grid center [*Smith*, 1999; *Ray*, 2007] in which the tidal solutions at a $0.25^o \times 0.25^o$ grid were simultaneously estimated. Radiational potential and free core nutation (FCN) resonance effects were also taken into account in this solution process [*Matsumoto et al*., 2000]. In addition, no solution was attempted at those grid points where only Envisat data are available.

It should be noted that some of the ocean tide models included tide gauge (and altimetry) data either as constraints (or assimilated into hydrodynamic models to compute ocean tides) or directly used the data to estimate tides. Thus the evaluation using ground-truth tide gauges may not be completely independent for some of the models, e.g., FES2004 or the TPXO models. In addition, the empirical models which used these models, e.g., EOT08a model used FES2004 as the 'reference' model, would have much higher spatial resolution and better coverage in coastal regions, as FES2004 model affords higher spatial resolutions than purely empirical ocean tide models.

3. Methods and Data Sets

Two methods were used for ocean tide model accuracy evaluation: (1) Reference ground truth (i.e. coastal and pelagic tidal constants) data analysis and (2) multiple mission altimetry sea level time series variance-reduction analysis. The first method involves the bilinear interpolation of the gridded model tidal constants to places where tidal records (from tide or bottom pressure gauges) are available, hence allowing the model tidal constants to be evaluated against the ground truth values. The evaluation was made by computing the RMS deviation of harmonic constants for each constituent *j* generated from an ocean tide model against the reference ground truth data, which is defined as:

$$RMS_j = \sqrt{\frac{1}{2N}\sum_{i=1}^{N}\left\{\left[h_1^{sol}(i,j) - h_1^{ref}(i,j)\right]^2 + \left[h_2^{sol}(i,j) - h_2^{ref}(i,j)\right]^2\right\}}$$

where $h_1^{sol}(i,j)$, $h_2^{sol}(i,j)$, $h_1^{ref}(i,j)$ and $h_2^{ref}(i,j)$ are the in-phase and quadrature amplitudes of ocean tide solution and the reference ground truth data respectively for each location *i* and constituent *j*, and *N* is the total number of locations where the in-phase and quadrature amplitudes are computed. Root Sum of Squares (RSS), which accounts for the total effect of 8 major constituents for each model against the reference ground truth data, is an indicator of the discrepancy of the model against the reference ground truth, and is defined as:

$$RSS = \sqrt{\sum_{j=1}^{8} RMS_j^2}$$

The Root Sum of Squares of the In-phase and Quadrature amplitudes for the reference ground truth data over 8 major constituents (RSSIQ) is also computed to assess the overall fraction of error of the ocean tide models against the ground truth data obtained from RSS, which is defined as:

$$RSSIQ = \sqrt{\frac{1}{2N}\sum_{j=1}^{8}\sum_{i=1}^{N}\left\{\left(h_1^{ref}(i,j)\right)^2 + \left(h_2^{ref}(i,j)\right)^2\right\}}$$

As a consequence, discrepancy D in percentage could be computed as RSS/RSSIQ×100%. Larger values of D indicate larger error in the tested ocean tide models against the ground truth data. Two sets of ground truth data had been provided by Richard D. Ray (personal communication) for this study: pelagic tidal constants at 102 sites and coastal tidal constants at 739 coastal sites. In this study, pelagic and coastal sites were selected where bilinear interpolation of model harmonic constants is possible for at least 7 major constituents. The sites

with records significantly different from the above ocean tide models were not used into the assessment, because either the tidal records are incorrect or the ocean tide models are unable to represent the ocean tides over the region.

The second method applies the tidal height prediction of ocean tide models in this study as a correction to the SSH anomaly for each altimeter data with the implicit assumption that a perfect ocean tide model leads to a minimum residual oceanographic variability, since tidal height change is the major signal in ocean [*King et al*., 1995]. Standard deviation of SSH anomaly and that of residual SSH anomaly after removal of tidal height predictions of ocean tide models along satellite tracks over the regions are computed to investigate how much the oceanographic variability be minimized after ocean tidal correction in this assessment. The residual SSH anomaly is defined as:

residual SSH anomaly = SSH anomaly – (diurnal + semidiurnal tides) – LP – seasonal signals

where the diurnal and semidiurnal tides are predicted by the ocean tide models, the equilibrium long-period tides (LP) are calculated based on *Cartwright and Edden* [1973] (which was adopted in GOT00.2 model) for consistency, the seasonal signals (i.e., annual and semi-annual) are estimated empirically from the SSH anomaly data corrected for the tidal height prediction of the FES2004 model.

Besides the aforementioned sea surface height (SSH) anomaly GDR data, those data from Jason-1 version c cycles 1–221 and from Jason-2 cycles 1–34 with improved precise orbit determination (POD) [*Desai*, 2009], sea state bias and wet troposphere corrections were utilized as independent data for the second assessment [*Dumont et al.*, 2008]. The abovementioned preprocessing step is also applied to those datasets.

4. RESULTS AND DISCUSSIONS

Seven coastal or shallow sea regions with high dynamic oceanic variability were selected in the tide model evaluation study. They are the Northwest Pacific, Northwest Atlantic, Gulf of Mexico, Patagonia Shelf, Southeast China, South Australia, and South Africa coastal regions. These regions are shown in Figures 1 through 7, with the standard deviation of residual multiple altimetry mission SSH anomaly using FES2004 model as the tide correction, together with locations of tide gauge sites with pelagic tidal constants used for tide model comparisons. The standard deviations of along satellite track points with magnitude larger than 1 m were eliminated from the figures.

The RMS differences of tidal constants of these models from in situ data along with RSS and RSSIQ at respective selected coastal sites over different regions (depicted with triangle symbol in the Figures) were computed (Table 1a and Table 1b). The percentage for the discrepancy D of the ocean tide models against the selected ground truth data, based on RSS and RSSIQ, were also calculated to assess the fraction of error. Comparison of this percentage among the ocean tide models reveal a strong disagreement between the ocean tide models and the tidal records at coastal sites, particularly in the Northwest Pacific and the Gulf of Mexico regions, where the disagreement exceeds 50%. The disagreement of other regions is, on the other hand, ~ 30% in general. This implies the tidal variability in shallow water is not well represented, for the ocean tide models studied.

The ocean tide models as compared with the coastal tide gauge records display heterogeneous performance over Southeast China and East Australia regions, showing different approaches in handling the regional hydrodynamics near the coast, such as different assumptions on dissipation and advection terms in handling the shallow water equations over a region, the bathymetry model to be used, the grading parameter to be chosen, and the least-squares adjust-

ment methodology. FES2004 and GOT00.2 models show a homogeneous performance over different selected regions, except Southeast China and East Australia regions. EOT08a and GOT4.7 model reproduces an improved result over FES2004 and GOT00.2 model, since EOT08a model is indeed based on FES2004 as a-priori model and GOT4.7 model is a successor of GOT00.2. In contrast, NAO.99b, TPXO6.2, TPXO7.1, and TPXO7.2 models exhibit inhomogeneous performance when compared with tidal records in coastal sites, depending on investigated regions. The OSU06 solution appears to have an average performance when compared to other ocean tide models as against the coastal tide gauge records.

Comparison of tidal constants of these models with in situ data at respective pelagic sites (depicted with star symbol in the Figures) was made in a similar fashion (Table 2a and Table 2b). Since no pelagic sites are found in Southeast China and South Africa regions, no statistics are shown in Table 2b. Comparison of the percentage for the disagreement reveals a relatively better agreement between the ocean tide models and the tidal records at pelagic sites than that at coastal sites, particularly in Northwest Pacific and Patagonia Shelf regions, where the disagreement is less than 5% in general. The ocean tide models as compared against the pelagic tide gauge records display homogeneous performance for all the regions selected in this investigation, except for the Gulf of Mexico and the Northwest Atlantic regions where OSU06 solution is performing worse in this study than other models. However, the pelagic sites in this study are situated at locations with strong ocean variability (i.e. loop current, the Gulf Stream) (Figure 2 & Figure 3). The same applies to one of two pelagic sites in East Australia. This is not surprising because neither the a-priori ocean tide model with built-in hydrodynamics nor hydrodynamic assimilation of tide gauge records and altimetry data is present in OSU06 solution as compared to other models. Thus, the FES2004 and GOT00.2 models have similar performance over all selected regions. In addition, the performance of the

EOT08a and GOT4.7 models are similar to the FES2004 and GOT00.2 models, respectively. In contrast, the performance of the NAO.99b model is worse when inter-compared with other models with hydrodynamic assimilation. It is indistinguishable which version of TPXO models could provide better result when compared with tidal records at pelagic sites, depending on investigated regions. An important comment is that pelagic sites are scarce in all the study regions. In particular and for example there is only 1 pelagic site in the Gulf of Mexico and the Northeast Atlantic ocean, respectively. As a result the analysis associated with pelagic data test in these sites could be statistically insignificant.

Because it is much clearer to explain high oceanic variability as displayed from the figures, summary of standard deviations of residual SSH anomaly before and after ocean tide corrections, with depth less than and greater than 1000 m, is displayed, respectively, in Table 3a through Table 4b. It can be shown that the SSH variability of shallow water areas of these regions is reduced by ~70% due to ocean tide corrections, except for the Gulf of Mexico (Table 3b) where ocean tide models present the least reduction of altimetry sea surface height variability (i.e. ~53%). On the contrary, most regions, except Northwest Pacific and Southeast China regions, show less than two-third of the variability explained by ocean tide corrections for the deep ocean SSH variance reduction study. This is mostly due to the areas with high standard deviations of residual SSH anomaly are in the western boundary current (e.g., Gulf Stream) (Figures 2, 3, 4, 6, and 7). The Gulf of Mexico presents the least reduction of SSH variability consistently in both shallow and deep oceans. The main cause of this result is the transport of warm water from Carribean Sea through Yucatan Channel that generates the loop current in the eastern Gulf (east of the ca. 272.5^{o}E longitude) [*Sheinbaum et al.*, 2002]. This loop current eventually spreads and forms anticyclonic (warm-core) eddies at the central of the Gulf (ca. 266 – 272.5^{o}E longitude) and their associated cyclonic (cold-core) eddies (ca.

west of 266°E longitude); these are the primary circulatory features of the region [*Davis et al.*, 2001] as could be seen from Figure 3 of this study and from Plate 3 of *Leben et al.* [1990] in which ocean tides had not been corrected for sea surface variability study using Geosat altimetry data. As a consequence, the interaction of ocean tides with the aforementioned non-tidal circulation features and possibly semi-diurnal and diurnal tidal mixing due to the shape of this ocean basin may not be able to be captured or separated from the time series of altimetry data and the global ocean tide models. The Gulf Stream in the Northwest Atlantic region, generated from the transport of the water from the Gulf of Mexico to Northwest Atlantic through the Straits of Florida, also explains why only ~47% of SSH variability is reduced by the ocean tide models. Overall, given the separation of deep and shallow water for the summary of standard deviations of residual SSH anomaly, the result shows consistency with the above pelagic tidal constants (both coastal and pelagic sites) comparison.

When the summary of standard deviation of residual SSH anomaly in shallow water (in Table 3a) and the percentage for the discrepancy of the ocean tide models against coastal tide gauge record (in Table 1a) in Northwest Pacific is compared, both results are inconsistent with each other. This difference is owing to the complicated estuary and canal system around this region where the tide gauge measurements for the ocean tides are confined by the coastlines and bathymetry. Figure 8 shows the M_2 tide from various ocean tide models in the Northwest Pacific coastal region with complicated estuary and canal systems. It displays different resolutions of each of the models, model coverage, and differences in amplitude. The coverage of EOT08a and FES2004 models is the best among models. It should be noted that the EOT08a model is very similar to FES2004 model, as EOT08a used FES2004 as a reference model for the empirical ocean tide modeling using multiple mission satellite altimetry data. Most of the models either possess larger M_2 amplitude or cover the estuary without tidal values. The dif-

ferences in amplitude within the estuary and canal system together with the model value coverage are quite high among different versions of TPXO models, whereas GOT00.2, GOT4.7 and OSU06 models show similar model coverage and values of amplitude despite different model resolutions. Overall, all models exhibit significant differences from one to another. This highlights the deficiency of most contemporary models to represent the ocean tides over coastal regions with complicated spatial configuration.

5. CONCLUSIONS

This paper provided an accuracy assessment of the ocean tide corrections (computed by the FES2004 and GOT00.2 models) in the Jason-2 Geophysical Data Record by evaluating these 2 models and 7 other historical and contemporary models, with a focus on selected coastal regions with high dynamic oceanic variability. The accuracy evaluation is conducted using reference ground truth data (pelagic tidal constants computed from tide or bottom pressure gauges, and coastal tide gauges) analysis and multiple satellite altimetry mission sea level time series variance reduction analysis. The result demonstrated consistent performance for all the contemporary ocean tide models, including the models used to compute ocean tide corrections on the Jason-2 GDR over all the selected coastal regions, and using both evaluation methods. The same applies to the EOT08a and GOT4.7 models in which the first model is based on FES2004 as a-priori model and the second model is the successor of GOT00.2 model. On the contrary, it is indistinguishable which version of TPXO models provides better performance. The accuracy of other models is regionally dependent as shown from the reference ground truth data analysis, particularly when compared to coastal tide gauge records. The purely empirical model (OSU06) shows better accuracy than any other models along the Northwest Atlantic, Southeast China and East Australia coasts. It should be noted that the tide gauge evaluation may not be independent for some of the tide models, as tide gauge data

were either used as constraints or were directly assimilated into hydrodynamic modeling leading to generation of these ocean tide models.

The consistent multiple satellite mission altimetry sea level time series variance reduction analysis for all the ocean tide models used in this study allows one to further explore the reduction of sea surface height variability over the selected coastal regions. It is concluded that the reduction of the sea surface height variability in the Gulf of Mexico is the least among all the selected coastal regions no matter in the shallow or deep ocean, because the loop current caused by the transport of warm water into the Gulf. The loop current variability complicates the interaction of the ocean tides with the non-tidal circulation features and possibly semi-diurnal and diurnal tidal mixing due to the shape of the ocean basin, which poses a difficulty for the purely empirical model to capture ocean tides accurately in the deep Gulf of Mexico as indicated by the ground truth data analysis (Table 2b). Due to the outflow of the Gulf of Mexico to the Northwest Atlantic Ocean, the purely empirical model in the deep Northwest Atlantic region also exhibits a larger discrepancy with pelagic observations, indicating the ocean tide signals are contaminated by the non-tidal circulation features. The reference ground truth data analysis along the coast and the multiple satellite mission altimetry sea level time series analysis contradict to each other in the Northwest Pacific region, which is explainable by the complicated estuary and canal system around this region as discussed in the result. This also highlights the inability of the current ocean tide models to accurately predict ocean tides over shallow water regions where complicated local hydrodynamic effects dominate. Nonetheless, the competitive accuracy of the newly developed pure empirical altimetry tide model (OSU06) along the coasts suggests that regional hydrodynamic tide models that assimilate altimetric tides may significantly improve ocean tides over these shallow regions, as already demonstrated in the Northwest Atlantic region [*Han et al*., 2010].

ACKNOWLEDGEMENTS

This research is partially support by grants from NASA's Physical Oceanography Program under the Ocean Surface Topography Mission (OSTM) projects (JPL 1356532, and U. Colorado 154-5322), from Hong Kong Research Grants Council (Grant No. PolyU 5184/06E/B-Q02D), and from Canadian Space Agency. TOPEX/POSEIDON, Jason-1 and Jason-2 altimetry data products are from NASA and CNES, via JPL PODACC and CNES Aviso. ERS-1/-2 and Envisat altimetry data are from ESA/ESRIN, and GFO altimetry data are provided by the US Navy, via NOAA's Laboratory for Satellite Altimetry. This research was carried out, in part, by the Jet Propulsion Laboratory (JPL), California Institute of Technology, under contract with the National Aeronautics and Space Administration (NASA). We thank the two anonymous reviewers for their constructive comments which resulted in an improved manuscript. We thank the ocean tidal modelers for providing their models, and Richard Ray for providing pelagic and coastal gauge tidal constants.

REFERENCES

Andersen, O. B. 1994. Ocean tides in the North Altantic and adjacent seas from ERS-1 altimetry. *J. Geophys. Res.* 99 (C11): 22557–22573.

Bosch, W., R. Savcenko, F. Flechtner, C. Dahle, T. Mayer-Gurr, D. Stammer, E. Taguchi, and P. Canceil. 2009. Residual ocean tide signals from satellite altimetry, GRACE, gravity fields, and hydrodynamic modelling. *Geophys. J. Int.* 99 (178): 1185–1192.

Cartwright, D. E. and A. C. Edden. 1973. Corrected tables of the tidal harmonics. *Geophys. J. Roy. Astron. Soc.* 33: 253–264.

Davis, R. W., J. G. Ortega-Ortiz, C. A. Ribic, W. E. Evans, D. C. Biggs, P. H. Ressler, R. B. Cady, R. R. Leben, K. D. Mullin, and B. Würsig. 2001. Cetacean habitat in the northern oceanic Gulf of Mexico. *Deep-Sea Res.* I 49: 121–142.

Desai, S. D. 2009. An introduction to GPS-OGDR-SSH product for OSTM/Jason-2. Ocean Surface Topography Science Team (OSTST) Meeting, Seattle, Washington.

Dumont, J. P., V. Rosmorduc, N. Picot, S. Desai, H. Bonekamp, J. Figa, J. Lillibridge, and R. Sharroo. 2008. OSTM/ Jason-2 Products Handbook, Issue 1.2.

Egbert G. D., and S. Y. Erofeeva. 2002. Efficient inverse modeling of the barotropic ocean tides. *J. Atmos. Ocean. Technol*. 19 (2): 183–204.

Escudier, P. and J. –L. Fellous. 2009. The Next 15 years of Satellite Altimetry: ocean surface topography constellation user requirements document. By Collecte Localization Satellites (CLS) and Orange Bleue Conseil.

Fang G., Y. Wang, Z. Wei, B. H. Choi, X. Wang, and J. Wang. 2004. Empirical cotidal charts of the Bohai, Yellow, and East China Seas from 10 years of TOPEX/Poseidon altimetry. *J. Geophys. Res.* 109: C11006, doi: 10.1029/2004JC002484.

Fu L-L., E. J. Christensen, C. A. Yamarone, M. Lefebvre, Y. Menard, M. Dorrer, and P. Escudier. 1994. TOPEX/POSEIDON mission overview. *J. Geophys. Res.* 99 (C12): 24369–24381.

Fu L-L. and A. Cazenave. 2001, Satellite altimetry and earth sciences: a handbook of techniques and applications. San Diego, Calif. ; London : Academic.

Han G. 2000. Three-dimensional modeling of tidal currents and mixing quantities over the Newfoundland Shelf. *J. Geophys. Res.*, 105(C5), 11407-11422.

Han, G., S. Paturi, B. deYoung, Y. Yi and C.K. Shum, 2010. A 3-D data-assimilative tide model of Northwest Atlantic. *Atmosphere-Ocean*, in press.

Inazu, D., T. Sato, S. Miura, Y. Ohta, K. Nakamura, H. Fujimoto, C. F. Larsen, and T. Higuchi. 2009. Accurate ocean tide modeling in southeast Alaska and large tidal dissipation around Glacier Bay. *J. Oceanogr.* 65: 335–347.

King, C., D. Stammer, and C. Wunsch. 1995. Tide model comparison at CPMO/MIT. Working paper for the TOPEX/POSEIDON science working team tide model study. Dept. of Earth, Atmos., and Planet. Sc., MIT.

Kruizinga, G. 1997. Validation and applications of satellite radar altimetry. PhD dissertation. University of Texas at Austin.

Leben, R. R., G. Born, J. D. Thompson, and C. A. Fox. 1990. Mean sea surface and variability of the Gulf of Mexico using geosat altimetry data. *J. Geophys. Res.* 95 (C3): 3025–3032.

Le Provost C., M. L. Genco, F. Lyard, P. Vincent, and P. Canceil. 1994. Spectroscopy of the world ocean tides from a finite element hydrodynamic model. *J. Geophys. Res.* 99 (C12): 24777–24797.

Lyard F., F. Lefevre, T. Letellier, and O. Francis. 2006. Modelling the global ocean tides: modern insights from FES2004. *Ocean Dyn.* 56 (5–6): 394–415.

Lyard, F., L. Roblou, F. Birol. 2009. Precise error budget for the altimeter-derived tidal constants (in shelf and coastal seas). Ocean Surface Topography Science Team (OSTST) Meeting, Seattle, Washington, USA.

Matsumoto K., T. Takanezawa, and M. Ooe. 2000. Ocean tide models developed by assimulating TOPEX/POSEIDON altimeter data into hydrodynamical model: A global model and a regional model around Japan. *J. Oceanogr.* 56: 567–581.

Ray, R. D. 1993. Global ocean tide models on the eve of TOPEX/POSEIDON. *IEEE Trans. Geosci. Remote Sens.* 31: 355–364.

Ray, R. D. 1999. A global ocean tide model from TOPEX/POSEIDON altimetry: GOT99.2. NASA Tech Memo – 209478.

Ray, R. D. 2007. Tidal analysis experiments with sun-synchronous satellite altimeter data. *J. Geod* 81: 247–257.

Ray, R. D. 2009. Tide correction errors. Ocean Surface Topography Science Team (OSTST) Meeting, Seattle, Washington.

Savcenko, R. and W. Bosch. 2008. EOT08a – empirical ocean tide model from multi-mission satellite altimetry. In: Report No. 81 Deutsches Geodätisches Forschungsinstitut (DGFI), München.

Sheinbaum J., J. Candela, A. Badan, and J. Ochoa. 2002. Flow structure and transport in the Yucatan Channel. *Geophys. Res. Lett.* 29 (3): 10.1029/2001GL013990.

Smith, A. J. E. 1999. Application of satellite altimetry for global ocean tide modeling. PhD Dissertation. Delft University Press.

Shum, C.K., P. L. Woodworth, O. B. Andersen, G. D. Egbert, O. Francis, C. King, S. M. Klosko, C. Le Provost, X. Li, J-M Molines, M. E. Parke, R. D. Ray, M. G. Schlax, D. Stammer, C. C. Tierney, P. Vincent, and C. I. Wunsch. 1997. Accuracy assessment of recent ocean tide models. *J. Geophys. Res.* 102 (C11): 25173–25194.

Shum, C. K., N. Yu, and C. S. Morris. 2001. Recent advances in ocean tidal science. *J. Geod. Soc. Japan* 47 (1): 528–537.

Shum, C.K., Y.C. Yi, H.K. Li, K. Matsumoto, T. Sato, X.C. Wang, Yi Chao, X.L. Deng, H. B. Iz. 2006. Coastal Ocean Tide Modeling Using Satellite Altimetry. Ocean Surface Topography Science Team (OSTST) Meeting, Venice, Italy.

Yi, Y., K. Matsumoto, C. K. Shum, Y. Wang, and R. Mautz. 2006. Advances in southern ocean tide modeling. *J. Geodyn.* 41: 128–132.

Yuan, L. G., X. L. Ding, P. Zhong, W. Chen, and D. F. Huang. 2009. Estimates of ocean tide loading displacements and its impact on position time series in Hong Kong using a dense continuous GPS network. *J. Geod.* doi: 10.1007/s00190-009-0319-0.

Zu, T., J. Gan, and S. Y. Erofeeva. 2008. Numerical study of the tide and tidal dynamics in the South China Sea. *Deep-Sea Research* I 55: 137–154.

Figure captions

Figure 1. Standard deviations of residual SSH anomaly at along satellite track locations and location of tide gauge sites used as the ground truth (pelagic sites shown as stars and coastal sites as triangles) with contour indicating the depth of ocean (positive upward in meters) in the Northwest Pacific region.

Figure 2. Standard deviations of residual SSH anomaly at along satellite track locations and location of tide gauge sites used as the ground truth (pelagic sites shown as stars and coastal sites as triangles) with contour indicating the depth of ocean (positive upward in meters) in the Northwest Atlantic region.

Figure 3. Standard deviations of residual SSH anomaly at along satellite track locations and location of tide gauge sites used as the ground truth (pelagic sites shown as stars and coastal sites as triangles) with contour indicating the depth of ocean (positive upward in meters) in the Gulf of Mexico region.

Figure 4. Standard deviations of residual SSH anomaly at along satellite track locations and location of tide gauge sites used as the ground truth (pelagic sites shown as stars and coastal sites as triangles) with contour indicating the depth of ocean (positive upward in meters) in Patagonia Shelf region.

Figure 5. Standard deviations of residual SSH anomaly at along satellite track locations and location of tide gauge sites used as the ground truth (pelagic sites shown as stars and coastal sites as triangles) with contour indicating the depth of ocean (positive upward in meters) in Southeast China region.

Figure 6. Standard deviations of residual SSH anomaly at along satellite track locations and location of tide gauge sites used as the ground truth (pelagic sites shown as stars and coastal sites as triangles) with contour indicating the depth of ocean (positive upward in meters) in East Australia region.

Figure 7. Standard deviations of residual SSH anomaly at along satellite track locations and location of tide gauge sites used as the ground truth (pelagic sites shown as stars and coastal sites as triangles) with contour indicating the depth of ocean (positive upward in meters) in South Africa region.

Figure 8. M2 tide of different ocean tide models in parts of the Northwest Pacific region. The parenthesis of EOT08a indicates FES2004 were used as a-priori background model.

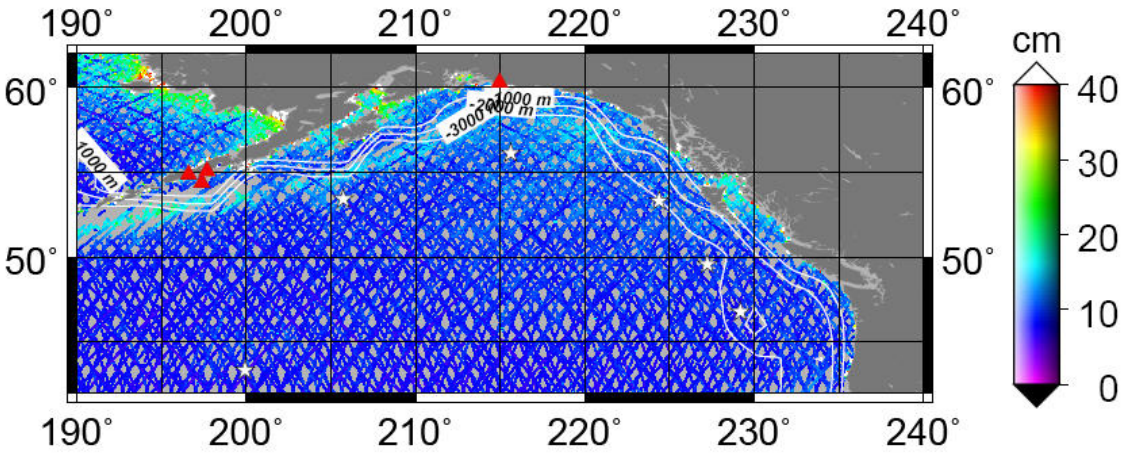

Figure 1.

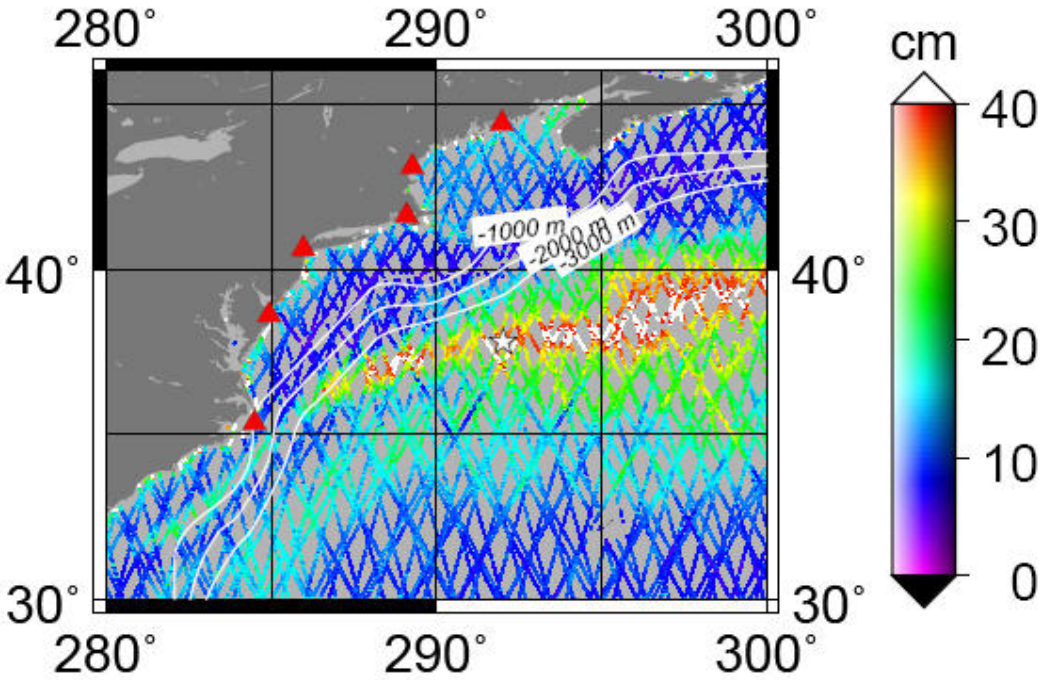

Figure 2.

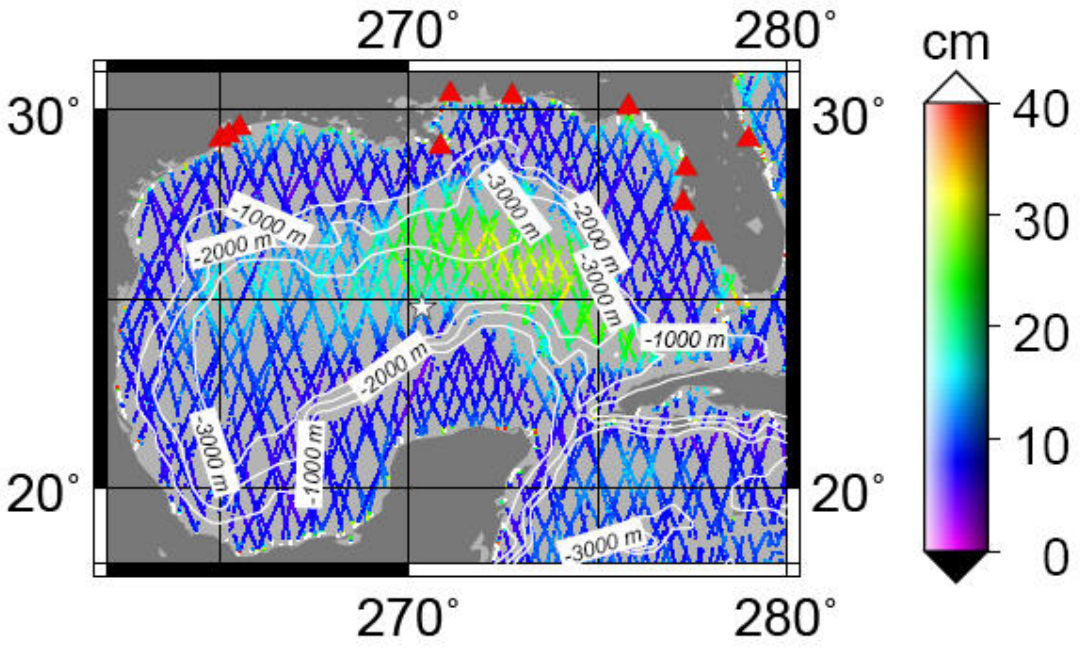

Figure 3.

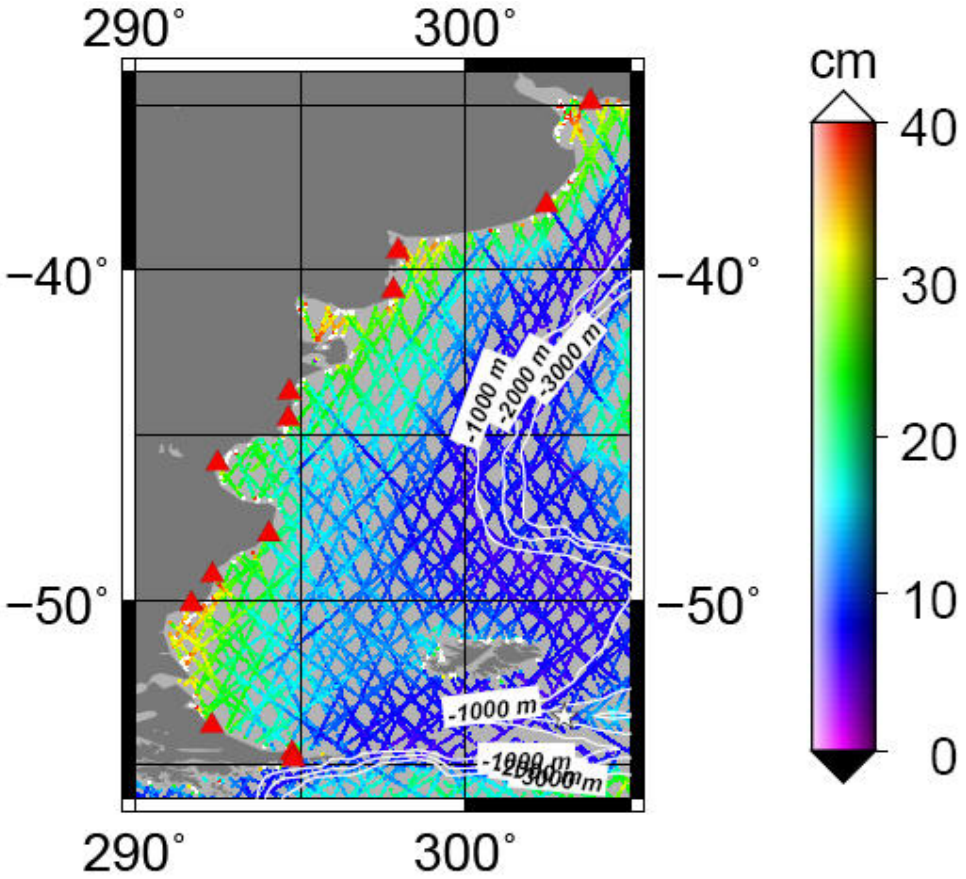

Figure 4.

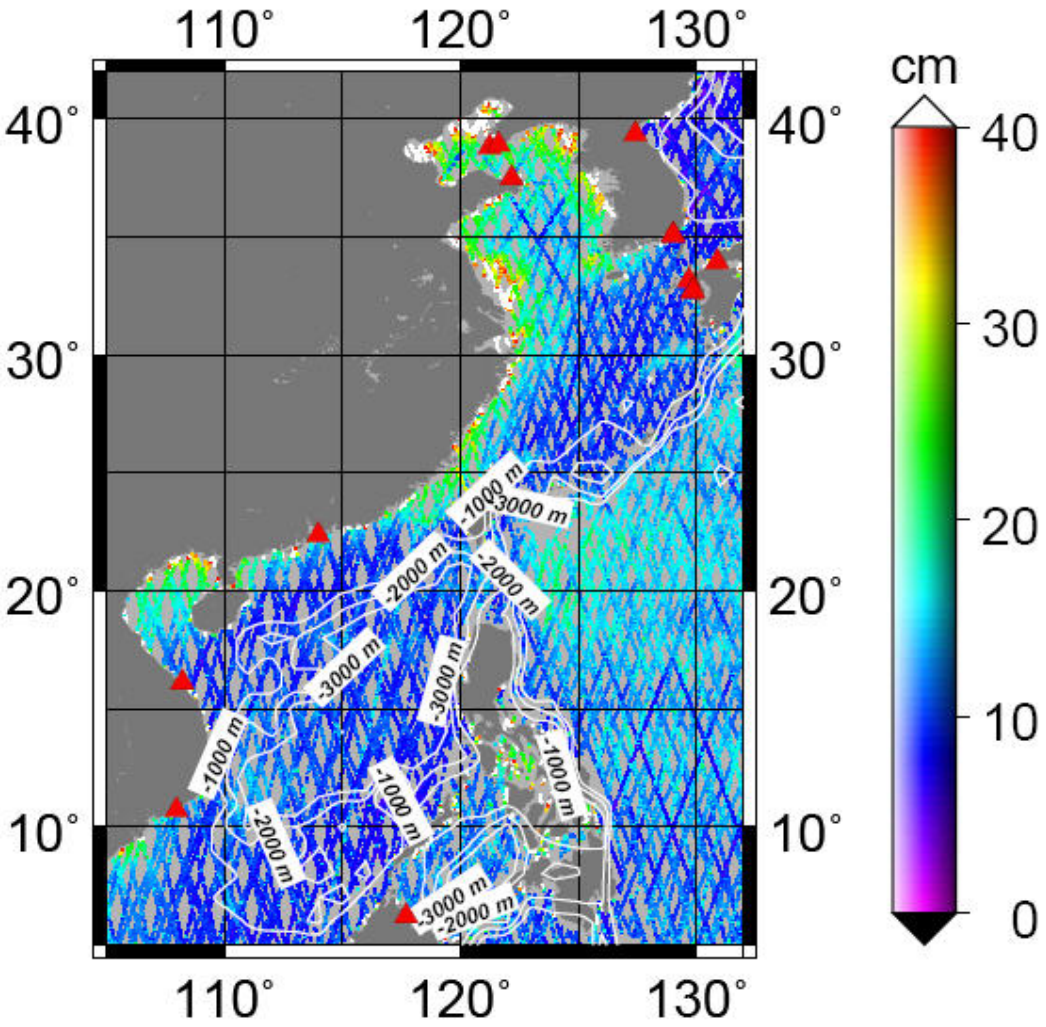

Figure 5.

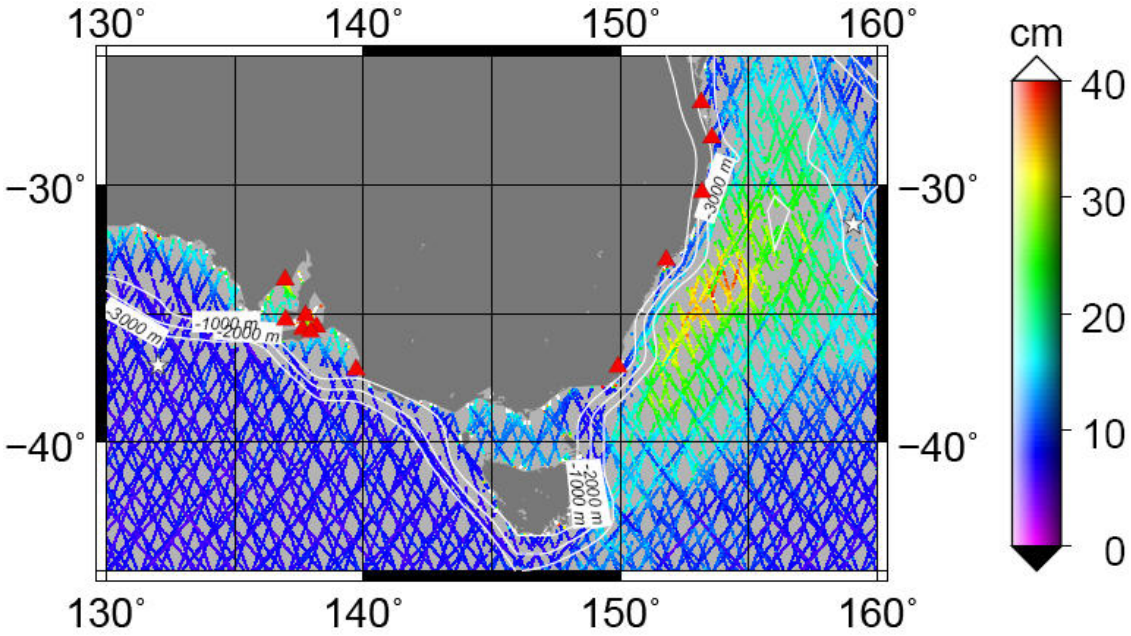

Figure 6.

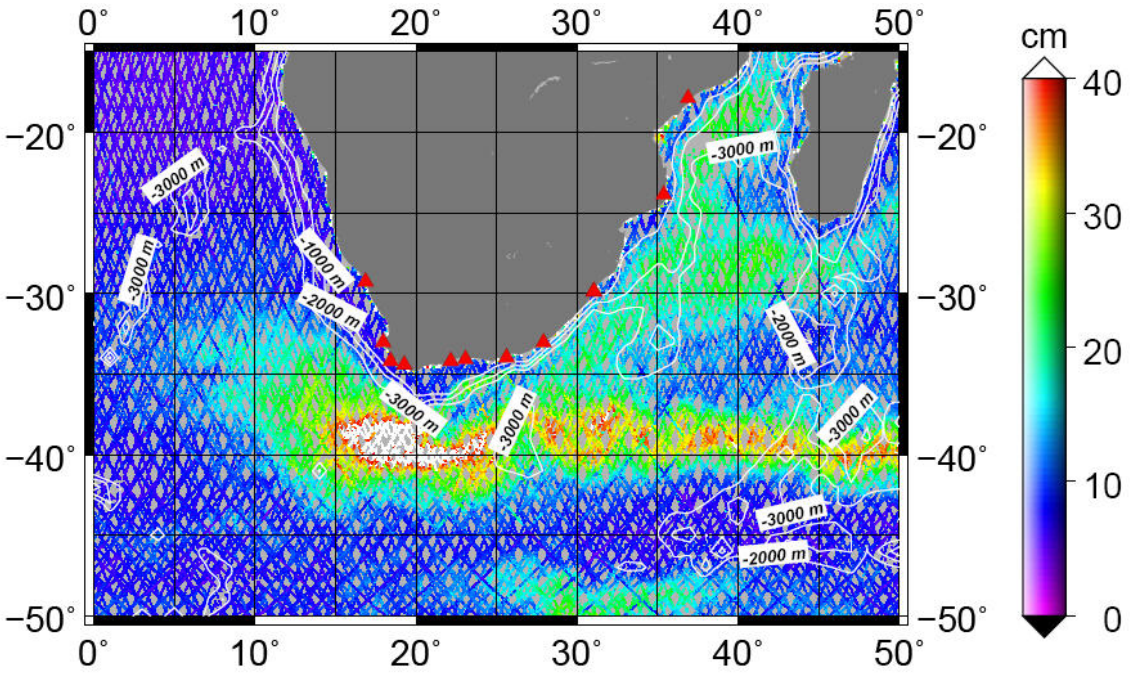

Figure 7.

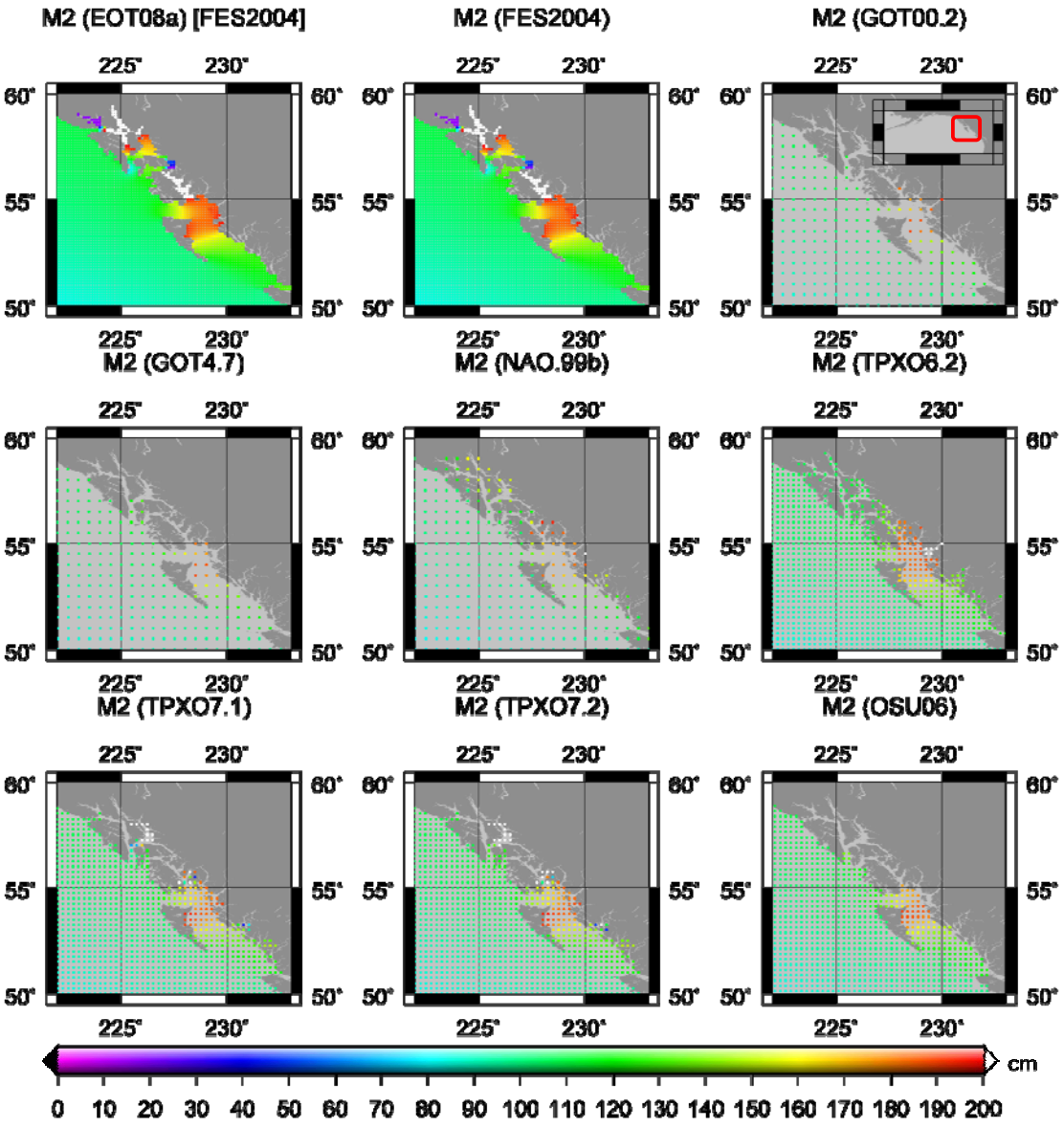
M2 (EOT08a) [FES2004]
M2 (FES2004)
M2 (GOT00.2)
M2 (GOT4.7)
M2 (NAO.99b)
M2 (TPXO6.2)
M2 (TPXO7.1)
M2 (TPXO7.2)
M2 (OSU06)
225° 230°
60° 55° 50°
cm
0 10 20 30 40 50 60 70 80 90 100 110 120 130 140 150 160 170 180 190 200

Figure 8.

Table 1a. Ground truth comparison of ocean tide models at coastal tide gauge stations (in cm). Note that D is the percentage value represents the disagreement of the ocean tide models against the ground truth data (i.e.RSS/RSSIQ×100%), with bold letters indicating the best model and OSU06 solution.

Model	M_2	S_2	K_1	O_1	N_2	P_1	K_2	Q_1	RSS	D (%)
Northwest Pacific (no. of tide gauges = 4) (RSSIQ = 48.94 cm)										
EOT08a	30.54	11.32	13.70	10.06	6.46	4.40	3.11	2.00	37.74	77.11
FES2004	30.83	11.12	13.80	10.25	6.34	4.59	2.87	2.01	37.99	77.63
GOT00.2	33.22	10.94	14.24	10.08	8.38	4.67	2.94	2.03	40.41	82.57
GOT4.7	29.35	10.45	13.69	9.89	5.43	4.47	2.79	2.01	36.29	74.15
NAO.99b	40.37	11.57	13.98	11.01	8.94	4.47	2.94	1.98	46.83	95.69
TPXO.6.2	28.97	10.63	13.15	9.98	5.39	4.11	2.90	1.99	35.82	**73.19**
TPXO.7.1	41.98	11.71	15.18	10.89	9.83	4.83	3.35	2.29	48.84	99.79
TPXO.7.2	42.03	11.50	15.23	10.90	9.99	4.85	3.33	2.29	48.88	99.88
OSU06	31.92	10.83	14.25	10.30	6.69	4.57	2.83	2.01	39.02	**79.73**

Table 1b. Ground truth comparison of ocean tide models at coastal tide gauge stations (in cm) showing RSS and D only, with bold letters indicating the best model and OSU06 solution over a particular region.

Model	Northwest Atlantic (no. of tide gauges = 6) (RSSIQ = 66.71 cm)		Gulf of Mexico (no. of tide gauges = 11) (RSSIQ = 21.55 cm)	
	RSS	D (%)	RSS	D (%)
EOT08a	14.37	21.54	10.57	**49.05**
FES2004	14.71	22.05	11.05	51.28
GOT00.2	14.40	21.59	11.78	54.66
GOT4.7	14.90	22.34	10.63	49.33
NAO.99b	28.00	41.97	12.84	59.58
TPXO.6.2	13.15	**19.71**	13.03	60.46
TPXO.7.1	16.51	24.75	11.96	55.50
TPXO.7.2	15.86	23.77	12.05	55.92
OSU06	12.17	**18.24**	12.42	**57.63**
Model	Patagonia Shelf (no. of tide gauges = 13) (RSSIQ = 137.10 cm)		Southeast China (no. of tide gauges = 14) (RSSIQ = 53.20 cm)	
	RSS	D (%)	RSS	D (%)
EOT08a	31.75	23.16	15.50	29.14
FES2004	30.92	**22.55**	15.72	29.55
GOT00.2	33.88	24.71	22.87	42.99
GOT4.7	34.18	24.93	22.86	42.97
NAO.99b	39.17	28.57	14.12	**26.54**
TPXO.6.2	46.82	34.15	16.53	31.07
TPXO.7.1	43.35	31.62	25.03	47.05
TPXO.7.2	38.01	27.72	20.20	37.97
OSU06	36.24	**26.43**	10.80	**20.30**
Model	East Australia (no. of tide gauges = 12) (RSSIQ = 36.55 cm)		South Africa (no. of tide gauges = 12) (RSSIQ = 53.55 cm)	
	RSS	D (%)	RSS	D (%)
EOT08a	15.70	42.95	17.15	32.03
FES2004	18.06	49.41	17.08	31.90
GOT00.2	19.68	53.84	17.32	32.34
GOT4.7	11.11	**30.40**	17.14	32.01
NAO.99b	16.97	46.43	17.24	32.19
TPXO.6.2	19.08	52.20	17.05	31.84
TPXO.7.1	14.23	38.93	16.40	**30.63**
TPXO.7.2	14.18	38.80	16.69	31.17
OSU06	9.80	**26.81**	17.76	**33.17**

Table 2a. Ground truth comparison of ocean tide models at pelagic tide gauge stations (in cm). Note that D is the percentage value represents the disagreement of the ocean tide models against the ground truth data (i.e.RSS/RSSIQ×100%), with bold letters indicating the best model and OSU06 solution.

Model	M_2	S_2	K_1	O_1	N_2	P_1	K_2	RSS	D (%)
	Northwest Pacific (no. of tide gauges = 6) (RSSIQ = 71.61 cm)								
EOT08a	1.70	1.55	1.56	1.26	1.36	0.41	0.79	3.46	4.83
FES2004	1.77	1.48	1.63	1.28	1.29	0.61	0.66	3.47	4.85
GOT00.2	1.65	1.53	1.47	1.30	1.20	0.45	0.66	3.31	**4.62**
GOT4.7	1.65	1.49	1.52	1.35	1.28	0.44	0.69	3.38	4.72
NAO.99b	3.07	1.51	2.69	2.00	1.43	0.72	0.68	5.09	7.11
TPXO.6.2	1.77	1.51	1.58	1.31	1.34	0.41	0.66	3.46	4.83
TPXO.7.1	1.61	1.53	1.55	1.33	1.36	0.37	0.70	3.40	4.74
TPXO.7.2	1.59	1.50	1.57	1.36	1.35	0.40	0.66	3.40	4.74
OSU06	1.69	2.47	1.59	1.29	1.09	0.44	0.61	3.86	**5.39**

Table 2b. Ground truth comparison of ocean tide models at pelagic tide gauge stations (in cm) showing RSS and D only, with bold letters indicating the best model and OSU06 solution over a particular region.

Model	Northwest Atlantic (no. of tide gauges = 1) (RSSIQ = 32.13 cm)		Gulf of Mexico (no. of tide gauges = 1) (RSSIQ = 15.06 cm)	
	RSS	D (%)	RSS	D (%)
EOT08a	1.63	5.07	1.93	12.82
FES2004	1.57	4.89	1.80	11.95
GOT00.2	1.47	4.58	1.55	10.29
GOT4.7	1.09	3.39	1.47	**9.76**
NAO.99b	3.02	9.40	1.89	12.55
TPXO.6.2	1.08	**3.36**	1.62	10.76
TPXO.7.1	1.26	3.92	1.81	12.02
TPXO.7.2	1.44	4.48	1.61	10.69
OSU06	5.29	**16.46**	4.73	**31.41**
Model	Patagonia Shelf (no. of tide gauges = 1) (RSSIQ = 31.36 cm)		East Australia (no. of tide gauges = 2) (RSSIQ = 36.07 cm)	
	RSS	D (%)	RSS	D (%)
EOT08a	1.11	3.54	3.13	8.68
FES2004	1.32	4.21	2.66	**7.37**
GOT00.2	0.71	**2.26**	3.13	8.68
GOT4.7	0.84	2.68	3.13	8.68
NAO.99b	2.94	9.38	3.04	8.43
TPXO.6.2	0.89	2.84	2.96	8.21
TPXO.7.1	0.89	2.84	3.14	8.71
TPXO.7.2	0.75	2.39	3.09	8.57
OSU06	1.16	**3.70**	4.47	**12.39**

Table 3a. Standard deviations of residual SSH anomaly of ocean tide models along satellite tracks in shallow ocean with depth less than 1000 m (in cm). Stdev (before) and Stdev (after) are the standard deviation of the SSH anomaly before and after ocean tide correction for the entire region. VE is the variance explained by ocean tide correction for the entire region, with bold letters indicating the best model and OSU06 solution. Note that Jason-1 (ver. c) and Jason-2 altimeter data were not included in the generation of the OSU06 solution.

Model	Altimeter data							Stdev (after)	VE (%)
	Topex/ Poseidon	Topex Interleave	GFO	Envisat	Jason-1 (ver. b)	Jason-1 (ver. c)	Jason-2		
Northwest Pacific (Stdev (before) = 169.67 cm)									
EOT08a	13.02	13.36	14.76	15.01	12.04	10.18	12.45	32.59	80.79
FES2004	13.90	13.89	15.30	15.48	12.40	10.66	12.95	33.93	80.00
GOT00.2	12.85	13.51	14.79	14.88	12.21	10.36	12.58	32.66	80.75
GOT4.7	12.51	13.20	14.39	14.71	12.06	10.21	12.25	32.02	**81.13**
NAO.99b	13.27	13.84	15.33	15.63	12.62	10.92	13.32	33.92	80.01
TPXO.6.2	13.78	13.98	15.35	15.93	12.22	10.44	13.09	34.02	79.95
TPXO.7.1	14.00	14.00	15.56	16.04	12.44	10.69	13.32	34.44	79.71
TPXO.7.2	13.48	13.67	15.15	15.58	12.30	10.51	13.00	33.57	80.22
OSU06	12.65	13.24	14.57	14.66	12.07	10.30	12.32	32.19	**81.03**

Table 3b. Standard deviations of residual SSH anomaly of ocean tide models along satellite tracks in shallow ocean with depth less than 1000 m (in cm) with Jason-1 (ver. c) and Jason-2 are shown. Stdev (before) and Stdev (after) are the standard deviation of the SSH anomaly before and after ocean tide correction for the entire region. VE is the variance explained by ocean tide correction for the entire region, with bold letters indicating the best model and OSU06 solution. Note that Jason-1 (ver. c) and Jason-2 altimeter data were not included in the generation of the OSU06 solution.

Model	Northwest Atlantic (Stdev (before) = 127.07 cm)				Gulf of Mexico (Stdev (before) = 56.14 cm)			
	Jason-1 (ver. c)	Jason-2	Stdev (after)	VE (%)	Jason-1 (ver. c)	Jason-2	Stdev (after)	VE (%)
EOT08a	9.14	10.93	28.18	**77.82**	7.73	11.81	26.49	52.82
FES2004	9.47	11.17	28.77	77.36	7.82	12.12	26.76	52.33
GOT00.2	9.40	11.03	28.66	77.45	7.75	11.44	26.28	53.19
GOT4.7	9.06	10.88	28.23	77.79	7.74	11.49	26.18	**53.37**
NAO.99b	9.36	11.60	29.89	76.48	7.85	11.71	26.72	52.41
TPXO.6.2	9.28	11.71	29.47	76.81	7.70	11.74	26.58	52.66
TPXO.7.1	9.21	11.39	28.86	77.29	7.83	11.71	26.75	52.35
TPXO.7.2	9.21	11.09	28.63	77.47	7.85	11.57	26.56	52.69
OSU06	9.00	10.86	27.77	**78.15**	7.66	11.25	25.65	**54.31**
Model	Patagonia Shelf (Stdev (before) = 167.60 cm)				Southeast China (Stdev (before) = 56.14 cm)			
	Jason-1 (ver. c)	Jason-2	Stdev (after)	VE (%)	Jason-1 (ver. c)	Jason-2	Stdev (after)	VE (%)
EOT08a	10.63	12.50	35.70	78.70	10.59	13.83	32.60	78.30
FES2004	11.54	13.67	37.58	77.58	14.08	17.32	39.10	73.98
GOT00.2	10.89	12.81	36.33	78.32	11.40	14.15	34.11	77.30
GOT4.7	10.62	12.50	35.46	**78.84**	10.53	13.33	31.90	**78.77**
NAO.99b	11.10	12.71	37.46	77.65	10.93	14.24	33.93	77.42
TPXO.6.2	11.14	13.31	37.60	77.56	12.18	15.38	38.17	74.60
TPXO.7.1	10.85	13.29	36.75	78.07	13.60	17.47	40.73	72.89
TPXO.7.2	10.67	12.56	35.99	78.53	12.75	16.24	37.68	74.92
OSU06	10.83	12.35	35.78	**78.65**	10.38	13.29	31.64	**78.94**
Model	East Australia (Stdev (before) = 103.42 cm)				South Africa (Stdev (before) = 125.26 cm)			
	Jason-1 (ver. c)	Jason-2	Stdev (after)	VE (%)	Jason-1 (ver. c)	Jason-2	Stdev (after)	VE (%)
EOT08a	8.96	14.93	30.87	70.16	9.11	15.94	28.83	76.99
FES2004	9.45	15.20	32.21	68.85	9.74	16.40	29.64	76.34
GOT00.2	9.01	15.11	31.84	69.22	8.68	15.63	28.30	77.41
GOT4.7	8.77	14.76	30.54	**70.47**	8.55	15.66	27.96	77.67
NAO.99b	9.02	15.24	31.99	69.07	8.63	15.70	28.72	77.07
TPXO.6.2	9.54	15.24	32.46	68.62	9.02	15.96	28.83	76.98
TPXO.7.1	8.85	14.75	31.28	69.76	8.47	15.57	28.34	77.38
TPXO.7.2	8.84	14.74	31.26	69.78	8.39	15.42	27.96	**77.68**
OSU06	8.93	14.83	30.36	**70.65**	8.58	15.77	28.00	**77.65**

Table 4a. Standard deviations of residual SSH anomaly of ocean tide models along satellite tracks in deep ocean with depth greater than 1000 m (in cm). Stdev (before) and Stdev (after) are the standard deviation of the SSH anomaly before and after ocean tide correction for the entire region. VE is the variance explained by ocean tide correction for the entire region, with bold letters indicating the best model and OSU06 solution. Note that Jason-1 (ver. c) and Jason-2 altimeter data were not included in the generation of the OSU06 solution.

Model	Altimeter data							Stdev (after)	VE (%)
	Topex/ Poseidon	Topex Interleave	GFO	Envisat	Jason-1 (ver. b)	Jason-1 (ver. c)	Jason-2		
Northwest Pacific (Stdev (before) = 156.53 cm)									
EOT08a	9.67	9.17	10.26	9.53	9.43	9.16	8.79	23.61	84.91
FES2004	9.66	9.22	10.30	9.52	9.50	9.25	8.98	23.71	84.85
GOT00.2	9.67	9.19	10.22	9.50	9.44	9.18	8.82	23.60	84.92
GOT4.7	9.63	9.20	10.25	9.53	9.45	9.19	8.81	23.62	**84.91**
NAO.99b	10.08	10.04	11.01	10.50	10.20	9.96	9.84	25.51	83.70
TPXO.6.2	9.69	9.23	10.30	9.69	9.46	9.20	8.65	23.75	84.83
TPXO.7.1	9.69	9.17	10.26	9.62	9.42	9.16	8.70	23.65	84.89
TPXO.7.2	9.68	9.12	10.22	9.58	9.39	9.13	8.82	23.57	84.94
OSU06	9.79	9.21	10.48	9.55	9.54	9.28	9.03	23.88	**84.74**

Table 4b. Standard deviations of residual SSH anomaly of ocean tide models along satellite tracks in shallow ocean with depth greater than 1000 m (in cm) with Jason-1 (ver. c) and Jason-2 are shown. Stdev (before) and Stdev (after) are the standard deviation of the SSH anomaly before and after ocean tide correction for the entire region. VE is the variance explained by ocean tide correction for the entire region, with bold letters indicating the best model and OSU06 solution. Note that Jason-1 (ver. c) and Jason-2 altimeter data were not included in the generation of the OSU06 solution.

Model	Northwest Atlantic (Stdev (before) = 90.03 cm)				Gulf of Mexico (Stdev (before) = 53.28 cm)			
	Jason-1 (ver. c)	Jason-2	Stdev (after)	VE (%)	Jason-1 (ver. c)	Jason-2	Stdev (after)	VE (%)
EOT08a	19.20	17.77	47.51	**47.22**	14.55	13.45	35.01	34.29
FES2004	19.20	17.75	47.55	47.19	14.59	13.46	35.05	34.21
GOT00.2	19.24	17.71	47.60	47.13	14.57	13.45	35.03	34.26
GOT4.7	19.23	17.71	47.57	47.16	14.55	13.44	34.98	**34.34**
NAO.99b	19.29	17.81	47.75	46.96	14.61	13.49	35.10	34.13
TPXO.6.2	19.22	17.70	47.58	47.15	14.56	13.43	35.00	34.31
TPXO.7.1	19.26	17.72	47.62	47.10	14.59	13.47	35.07	34.17
TPXO.7.2	19.24	17.72	47.60	47.12	14.59	13.51	35.06	34.19
OSU06	18.90	17.92	47.39	**47.36**	14.31	14.06	34.95	**34.40**
Model	Patagonia Shelf (Stdev (before) = 72.02 cm)				Southeast China (Stdev (before) = 103.74 cm)			
	Jason-1 (ver. c)	Jason-2	Stdev (after)	VE (%)	Jason-1 (ver. c)	Jason-2	Stdev (after)	VE (%)
EOT08a	11.53	11.09	28.41	60.55	11.42	10.78	29.27	71.79
FES2004	11.55	11.09	28.49	60.43	11.52	10.93	29.56	71.51
GOT00.2	11.53	11.16	28.58	60.31	11.49	10.87	29.55	71.52
GOT4.7	11.51	11.09	28.40	60.57	11.42	10.78	29.24	**71.82**
NAO.99b	11.73	11.32	28.91	59.85	12.02	11.38	30.69	70.42
TPXO.6.2	11.51	11.08	28.39	**60.58**	11.64	11.06	29.61	71.46
TPXO.7.1	11.53	11.10	28.43	60.53	11.58	10.93	29.61	71.46
TPXO.7.2	11.56	11.15	28.50	60.42	11.54	10.89	29.48	71.58
OSU06	11.21	10.93	27.77	**61.44**	11.36	10.81	29.10	**71.95**
Model	East Australia (Stdev (before) = 87.75 cm)				South Africa (Stdev (before) = 95.01 cm)			
	Jason-1 (ver. c)	Jason-2	Stdev (after)	VE (%)	Jason-1 (ver. c)	Jason-2	Stdev (after)	VE (%)
EOT08a	13.45	11.86	32.93	**62.48**	15.81	13.05	38.86	**59.09**
FES2004	13.53	11.92	33.08	62.30	15.85	13.10	38.95	59.01
GOT00.2	13.49	11.92	33.01	62.38	15.85	13.06	38.94	59.01
GOT4.7	13.45	11.84	32.92	**62.48**	15.84	13.06	38.91	59.05
NAO.99b	13.58	12.01	33.21	62.15	15.95	13.15	39.26	58.67
TPXO.6.2	13.47	11.88	32.94	62.46	15.83	13.03	38.91	59.05
TPXO.7.1	13.46	11.86	32.94	62.46	15.83	13.04	38.91	59.05
TPXO.7.2	13.46	11.87	32.96	62.44	15.83	13.04	38.91	59.05
OSU06	13.57	12.19	33.03	**62.35**	15.83	13.23	38.74	**59.22**